LBNL-43560
BNL-HET-99/15
ATL-COM-PHYS-99-017
July, 1999

Measurements of Masses in SUGRA Models at LHC[1]

Henri Bachacou[a,c], Ian Hinchliffe[a] and Frank E. Paige[b]
[a] *Lawrence Berkeley National Laboratory, Berkeley, CA*
[b] *Brookhaven National Laboratory, Upton, NY*
[c] *Kungliga Tekniska Högskolan, Stockholm, Sweden*

Abstract

This paper presents new measurements in a case study of the minimal SUGRA model with $m_0 = 100\,\mathrm{GeV}$, $m_{1/2} = 300\,\mathrm{GeV}$, $A_0 = 0$, $\tan\beta = 2$, and $\operatorname{sgn}\mu = +$ based on four-body distributions from three-step decays and on minimum masses in such decays. These measurements allow masses of supersymmetric particles to be determined without relying on a model. The feasibility of testing slepton universality at the $\sim 0.1\%$ level at high luminosity is discussed. In addition, the effect of enlarging the parameter space of the minimal SUGRA model is discussed. The direct production of left handed sleptons and the non-observation of additional structure in the dilepton invariant mass distributions is shown to provide additional constraints.

[1]This work was supported in part by the Director, Office of Science, Office of Basic Energy Research, Division of High Energy Physics of the U.S. Department of Energy under Contracts DE-AC03-76SF00098 and DE-AC02-98CH10886.

Contents

1 Introduction

If SUSY particles exist at the TeV mass scale, they will be produced at the LHC with large rates, so discovery of their existence will be straightforward. In minimal SUGRA [1] and similar models, however, the decay products of each SUSY particle contain an invisible lightest SUSY particle (LSP) $\tilde{\chi}_1^0$, so no masses can be reconstructed directly. Previous studies of SUGRA models have concentrated upon extracting information from kinematic end points measured in three-body final states [2, 3, 4, 5, 6] resulting from decays of the type $\tilde{\chi}_2^0 \to \tilde{\chi}_1^0 \ell^+\ell^-$ and $\tilde{q}_L \to \tilde{\chi}_2^0 q \to h\tilde{\chi}_1^0 q$. Studies of GMSB [7, 8] models have shown that multi-step decay chains such as $\tilde{\chi}_2^0 \to \tilde{\ell}_R^\pm \ell^\mp \to \tilde{\chi}_1^0 \ell^+\ell^- \to \tilde{G}\gamma\ell^+\ell^-$ can provide multiple constraints which can be used to extract masses without fitting to any underlying model.

In this paper we exploit multi-step decays for SUGRA models, specifically the decay

$$\tilde{q}_L \to \tilde{\chi}_2^0 q \to \tilde{\ell}^\pm \ell^\mp \to \tilde{\chi}_1^0 \ell^+\ell^- q \qquad (1)$$

for the minimal SUGRA model with the previously studied [2, 6] parameters $m_0 = 100\,\mathrm{GeV}$, $m_{1/2} = 300\,\mathrm{GeV}$, $A_0 = 300\,\mathrm{GeV}$, $\tan\beta = 2$, and $\mathrm{sgn}\,\mu = +$. The masses for this point are given in Table 1. As we shall show below, we are able to reconstruct both upper edges for the $\ell^+\ell^-$, $\ell^+\ell^- q$, and $\ell^\pm q$ mass distributions and a lower edge for the $\ell^+\ell^- q$ mass coming from backwards decays of the $\tilde{\chi}_2^0$ in the $\tilde{q}_L$ rest frame. (The use of analogous upper and lower edges to reconstruct masses has been extensively discussed for e^+e^- colliders [9].) These measurements make it possible to reconstruct all the masses involved in the decay. As part of this analysis we develop a fitting procedure to make estimates of the statistical errors of the various measurements that are more quantitative than previous ones [2, 6].

We then illustrate how these and other techniques can be used to over-constrain the parameters of the minimal SUGRA model and place constraints on the model itself. As part of this study we will show how some signals change qualitatively as one varies the relations between the squark and slepton masses that the minimal SUGRA model predicts. We allow for the masses of the third generation squarks and sleptons to vary and for the masses of the sfermions in the $\mathbf{5}$ and $\mathbf{10}$ representations of $SU(5)$ to differ. This is the first step in assessing how well more general supersymmetric models can be constrained using data from the LHC.

The analyses presented here are based large samples of events (the actual numbers are given below) generated using ISAJET [10] and RUNDST 5, which implements a simple detector simulation [2, 8] including efficiencies representative of the ATLAS detector. Jets were found using a fixed cone algorithm of size $R = 0.4$. Missing energy was determined including the η coverage and a Gaussian approximation to the energy resolution of the calorimeter. Leptons energy resolutions were also included (for details see Ref. [8]) and an appropriate detector efficiency of 90% was included. The event selection cuts make the Standard Model background small compared to the SUSY signal, so that clean SUSY samples can be studied. In an actual experiment, the cuts are likely to be less severe so that more signal events will survive. The dominant background with our cuts is combinatorial background in the interesting SUSY events and other SUSY events that happen to pass the cuts.

This paper contains treats several distinct but closely related topics. Section 2 describes the extraction of combination of masses from four-body kinematic limits. Section 3 describes the use of a lower edge to determine another combination of masses, and Section 4 combines these measurements to determine several masses of SUSY particles without relying on a model fit. Section 5 discusses the errors that could be achieved on the dilepton endpoint. We already know [2, 6] that this error is quite small, but as precise a measurement as possible is useful as a test of e/μ universality.

Table 1: Masses of the superpartners, in GeV in the default case (Point 5) and in two modified cases with $m_5 = 75\,\mathrm{GeV}$ and $m_5 = 125\,\mathrm{GeV}$ described in Section 6. The first and second generation of squarks and sleptons are degenerate and so are not listed separately.

Superpartner	default	$m_5 = 75$ GeV	$m_5 = 125$ GeV
$\widetilde{g}$	769	769	769
$\widetilde{\chi}_1^\pm$	232	232	232
$\widetilde{\chi}_2^\pm$	523	525	520
$\widetilde{\chi}_1^0$	122	122	122
$\widetilde{\chi}_2^0$	233	233	233
$\widetilde{\chi}_3^0$	502	504	500
$\widetilde{\chi}_4^0$	526	528	524
$\widetilde{u}_L$	687	687	687
$\widetilde{u}_R$	664	664	664
$\widetilde{d}_L$	690	690	690
$\widetilde{d}_R$	662	659	666
$\widetilde{t}_1$	496	496	495
$\widetilde{t}_2$	706	706	705
$\widetilde{b}_1$	635	635	634
$\widetilde{b}_2$	662	659	666
$\widetilde{e}_L$	239	229	250
$\widetilde{e}_R$	157	157	157
$\widetilde{\nu}_e$	230	221	242
$\widetilde{\tau}_1$	157	157	157
$\widetilde{\tau}_2$	239	230	250
$\widetilde{\nu}_\tau$	230	220	242
h^0	95	95	95
H^0	616	613	618
A^0	610	608	613
$H^\pm$	616	613	619

Section 6 explores additional signatures that are relevant to some simple extensions of the minimal SUGRA model. Section 7 reexamines the global fits of parameters both for the minimal SUGRA model and for its extensions. Finally, after some concluding remarks, the appendix describes an unsuccessful attempt at full reconstruction of SUSY events.

2 Information from four-body decays

In this and the following two sections (3, 4) and in the Appendix, the analysis is based on a sample of 10^6 SUSY events generated with ISAJET 7.32. This sample corresponds to approximately 70 fb^{-1} of integrated luminosity. This large sample is needed so that the the statistical fluctuations shown on the plots in the these sections corresponds approximately to those expected in the actual data from one year at the LHC design luminosity. The Standard Model background is not included on the plots (generating comparable statistics for this is a prohibitive task) but is known to be small in the channels [2, 6] that are used in these sections.

Previous work on measurements in SUGRA models relied mainly on end points measured in three-body final states with one invisible particle [2, 3, 4, 5, 6]. It was subsequently found [8] in studying GMSB Point G1a that four-body distributions from multi-step decays such as $\tilde{\chi}_2^0 \to \tilde{\ell}_R^{\pm}\ell^{\mp} \to \tilde{\chi}_1^0 \ell^+\ell^- \to \tilde{G}\gamma\ell^+\ell^-$ contain even more information. This method has considerable generality as we now illustrate by applying it to the decay chain given in Equation 1 above. The three observed particles, ℓ^+, ℓ^- and q (which appears as a hadronic jet) can be used to make several mass distributions: $\ell^+\ell^- q$, ℓq and $\ell^+\ell^-$. The last distribution was considered previously [2, 6] and has a sharp kinematic end point that results when the unobserved $\tilde{\chi}_1^0$ momentum is minimized in the rest frame of $\tilde{\ell}_R^{\pm}$.

In order to ensure a clean sample of SUSY events the following event selection was applied.

- At least four jets with $p_{T,1} > 100\,\mathrm{GeV}$ and $p_{T,2,3,4} > 50\,\mathrm{GeV}$, where the jets are numbered in order of decreasing p_T.
- $M_{\mathrm{eff}} > 400\,\mathrm{GeV}$, where M_{eff} is the scalar sum of the transverse momenta of the four leading jets and the missing transverse energy:

$$M_{\mathrm{eff}} = p_{T,1} + p_{T,2} + p_{T,3} + p_{T,4} + \not{E}_T\,.$$

- $\not{E}_T > \max(100\,\mathrm{GeV}, 0.2 M_{\mathrm{eff}})$.
- Two isolated leptons of opposite charge with $p_T > 10\,\mathrm{GeV}$, $|\eta| < 2.5$. Isolation being defined so that there is less than 10 GeV of additional transverse energy in an $R = 0.2$ cone centered on the lepton.

With these cuts the Standard Model background is negligible, as can be seen from Figure 26 of Reference 2. Thus, Standard Model backgrounds will not be shown here.

It is expected that the two hardest jets will be those coming directly from $\tilde{q}_L \to \tilde{\chi}_2^0 q$ as a dominant production procees is that which leads to $\tilde{q}_L\tilde{g}$ and hence to pairs of $\tilde{q}_L$. Therefore, the smaller of the two masses formed by combining the leptons with one of the two highest p_T jets should be less than the four-body kinematic end point for squark decay, namely

$$M_{\ell\ell q}^{\max} = \left[\frac{\left(M_{\tilde{q}_L}^2 - M_{\tilde{\chi}_2^0}^2\right)\left(M_{\tilde{\chi}_2^0}^2 - M_{\tilde{\chi}_1^0}^2\right)}{M_{\tilde{\chi}_2^0}^2}\right]^{1/2} = 552.4\,\mathrm{GeV}\,.$$

The distribution of the smaller $\ell^+\ell^- q$ mass is plotted in Figure 1 with same-flavor lepton pairs weighted positively and opposite-flavor ones weighted negatively. The $e^+e^- + \mu^+\mu^- - e^{\pm}\mu^{\mp}$ combination cancels all contributions from two independent decays (assuming e-μ universality) and strongly reduces the combinatorial background. This distribution should vanish linearly as the end point is approached. Figure 1 also shows a linear fit near the end point. The extrapolation of this fit gives an end point of 568.0 GeV, 3.4% above the nominal value. The distribution itself is quite linear, so varying the interval over which the fit was made produces only small changes in the end-point value.

An additional selection was then made: one $\ell^+\ell^- q$ mass was required to less than 600 GeV and the other greater, so that the assignment of the jet to combine with the lepton pair is unambiguous. The combination with the smaller mass is then used for further analysis. The mass distribution of the $\ell^{\pm} q$ sub-system was then calculated for each lepton and the selected jet. If the jet mass is

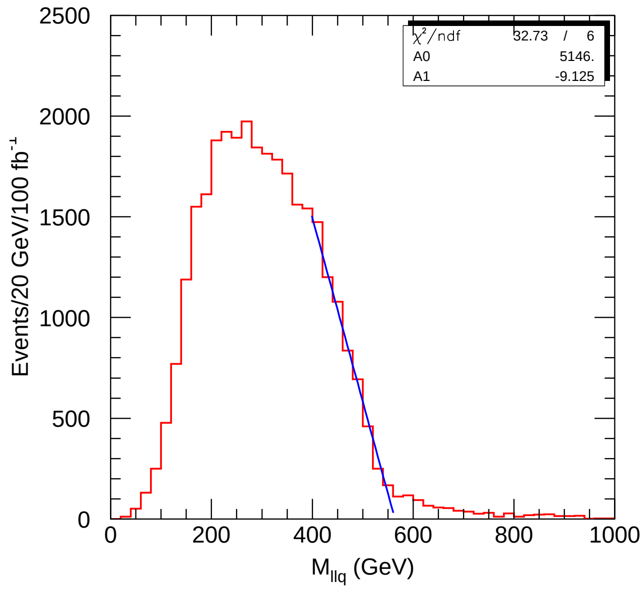

Figure 1: Mass distribution for the smaller of the two $\ell^+\ell^- q$ masses showing a linear fit near the four-body end point.

neglected, then the mass for the jet and the first lepton emitted has an end point analogous to the $\ell^+\ell^-$ one at

$$M_{\ell q}^{\max} = \left[\frac{\left(M_{\tilde{q}_L}^2 - M_{\tilde{\chi}_2^0}^2\right)\left(M_{\tilde{\chi}_2^0}^2 - M_{\tilde{\ell}_R}^2\right)}{M_{\tilde{\chi}_2^0}^2} \right]^{1/2} = 479.3\,\mathrm{GeV}$$

In order to make the former structure as clear as possible, the combination with the larger invariant mass out of the two possible $\ell^\pm q$ pairings in the $\ell^+\ell^- q$ combination is used in making Figure 2. Again events entered the histogram weighted by flavor ($+1$ for e^+e^- and $\mu^+\mu^-$ events and -1 for $e^\pm\mu^\mp$) in order to reduce combinatorial background.

There is also an end point where the spectrum vanishes for $M_{\ell q}$ formed using the lepton originating from the last step in the decay chain, Equation 1, at

$$M_{\ell q}^{\prime\max} = \left[\frac{\left(M_{\tilde{q}_L}^2 - M_{\tilde{\chi}_2^0}^2\right)\left(M_{\tilde{\ell}_R^0}^2 - M_{\tilde{\chi}_1^0}^2\right)}{M_{\tilde{\chi}_2^0}^2} \right]^{1/2} = 274.5\,\mathrm{GeV}\,.$$

The structure from this end point is buried under former distribution and hence is not visible. (In the GMSB case studied previously [8], the analogs of both end points were visible.)

If the resolution were perfect and there were no selection cuts, the ℓq mass distribution for the lepton emerging from the second step in the decay chain would be given by

$$M_{\ell q}^{\max}\sqrt{\frac{1+z}{2}}\,dz, \quad -1 < z < 1$$

where $M_{\ell q}^{max}$ is the end point given above and $z = \cos\theta^*$ is the cosine of the decay angle of the slepton in its rest frame. In order to determine whether the selection cuts or resolution are more responsible for the distortion and to estimate how well this end point might be measured, this form

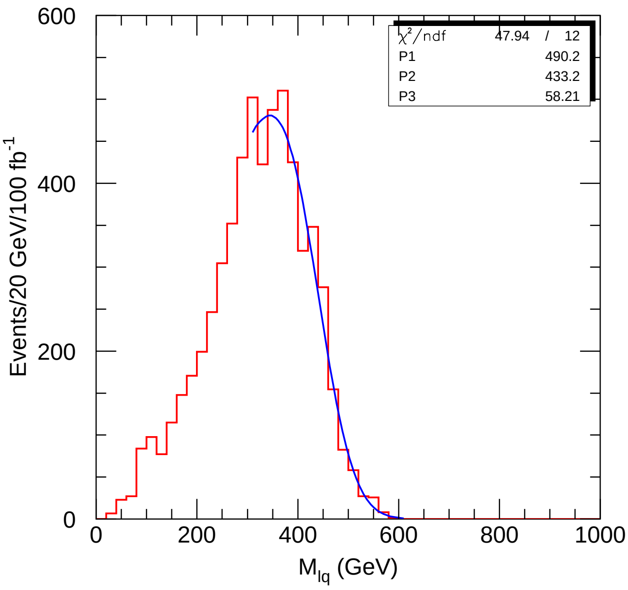

Figure 2: Distribution of the larger of the two $\ell^{\pm}q$ masses for $\ell^+\ell^-q$ events in which $M_{\ell\ell q} < 600\,\mathrm{GeV}$ and a fit described in the text.

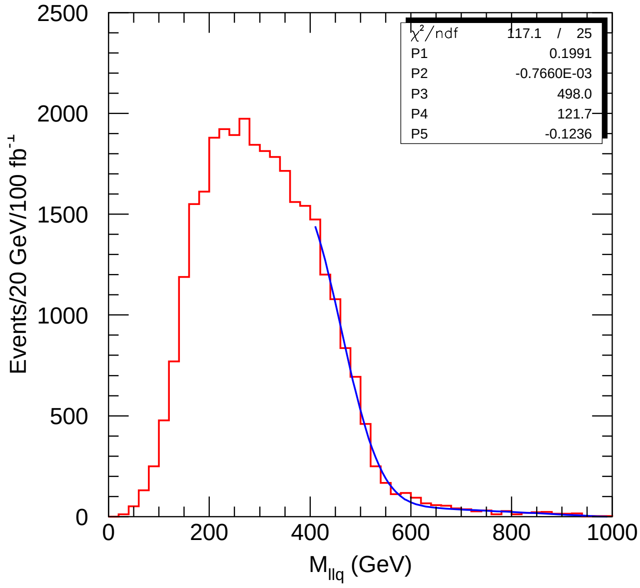

Figure 3: Distribution for the smaller of the two $\ell^+\ell^-q$ masses from Figure 1; a Gaussian-smeared fit plus a linear background described in the text is also shown.

was smeared with a Gaussian in an attempt to parametrise the resolution effects. The fit function is

$$f(M) = \int_{-1}^{+1} dz\, A \exp\left[\frac{1}{2\sigma^2}\left(M - M_{\ell q}^{\max}\sqrt{\frac{1+z}{2}}\right)^2\right]$$

with parameters A, $M_{\ell q}^{\max}$, and σ. The integral was done numerically using 96-point Gaussian quadrature integration, and the fit to Figure 2 was made using MINUIT and MINOS [11] inside PAW. The resulting fit, shown in Figure 2, gives $M_{\ell q}^{\max} = 433.2^{+3.2}_{-3.3}\,\mathrm{GeV}$, which is 9.6% lower than the true position and $\sigma = 58.2\,\mathrm{GeV}$. It has a reasonable χ^2, indicating that the cuts do not significantly distort the shape of the distribution over the fitted range. The shift to lower values is due primarily to energy lost out of the $R = 0.4$ jet cone. If the analysis is repeated with $R = 0.7$ jet cone it is about 3.8% low. The resolution is due mainly to the resolution on the jet energy measurement and is consistent with that expected given the form of our detector simulation.

The resolution smearing will also shift the position of the $\ell\ell q$ end point. This distribution was re-fit using the empirical form

$$f(M) = \int_0^{M_{\ell\ell q}} dz\, \left(a_1(M_{\ell\ell q} - z) + a_2(M_{\ell\ell q} - z)^2\right) \exp\left[\frac{1}{2\sigma^2}(M - z)^2\right] + b_1 + b_2 M$$

using the same σ obtained above and fitting for a_i, b_i, and $M_{\ell\ell q}$. This fit is shown in Figure 3 and gives $M_{\ell\ell q} = 498.0^{+7.2}_{-6.4}\,\mathrm{GeV}$, which is 9.8% low. The $R = 0.7$ jet cone gave a value that was 4.7% low. In an actual experiment these shifts due to energy loss out of the cone could be understood by using detailed comparisons of Monte Carlo simulations with data and using jets of known energy to set the jet energy scale [12].

The ratio of the ℓq and $\ell\ell q$ end points is independent of $M_{\tilde{q}_L}$:

$$\frac{M_{\ell q}}{M_{\ell\ell q}} = \sqrt{\frac{M_{\tilde{\chi}_2^0}^2 - M_{\ell_R}^2}{M_{\tilde{\chi}_2^0}^2 - M_{\tilde{\chi}_1^0}^2}} = 0.868\,,$$

compared with a fitted value of $433.2/498.0 = 0.870$ for the fits obtained using resolution smearing. This ratio should be less sensitive to the jet energy scale and so measured more accurately than the individual end points. The difference between the fitted and computed values is very small and the result is stable; repeating the same analysis using jets defined with an $R = 0.7$ cone shifts the individual fitted edges by $\sim 5\%$ but gives 0.877 for the ratio.

3 Lower edges

The upper limit of kinematic distributions has been used in the previous section to extract information. Kinematic distributions can also have lower limits. These have been exploited for example in the NLC SUSY analysis [9]. For a process like $e^+e^- \to \tilde{\mu}^+\tilde{\mu}^- \to \mu^+\tilde{\chi}_1^0\mu^-\tilde{\chi}_1^0$, the fixed center of mass energy and resulting fixed momentum of the $\tilde{\mu}$ results in a maximum and minimum energy of the observed muon which can be used to extract both $\tilde{\mu}$ and $\tilde{\chi}_1^0$ masses.

A similar analysis can be used for the process given in Equation 1 at the LHC. The squark mass plays a role analogous the center of mass energy in the e^+e^- case and a Lorentz invariant quantity must be used. For a given value of $z = \cos\theta^*$, the decay angle of the second lepton in the $\tilde{\chi}_2^0$ rest frame, the $\ell^+\ell^-$ mass is determined to be

$$M_{\ell\ell}^2 = (M_{\ell\ell}^{\max})^2\,\frac{1+z}{2}\,,$$

where

$$M_{\ell\ell}^{\max} = \sqrt{\frac{(M_2^2 - M_e^2)(M_e^2 - M_1^2)}{M_e^2}}\,.$$

There is a corresponding momentum $p_{\ell\ell}$ in the $\tilde{\chi}_2^0$ rest frame. Thus as a function of z there is a minimum of the $M_{\ell\ell q}$ mass. For $z = 0$ the expression for this minimum simplifies to

$$\begin{aligned}
(M_{\ell\ell q}^{\min})^2 &= \tfrac{1}{4M_2^2 M_e^2}\times \\
&\Big[-M_1^2M_2^4 + 3M_1^2M_2^2M_e^2 - M_2^4M_e^2 - M_2^2M_e^4 - M_1^2M_2^2M_q^2 - \\
&\quad M_1^2M_e^2M_q^2 + 3M_2^2M_e^2M_q^2 - M_e^4M_q^2 + (M_2^2 - M_q^2)\times \\
&\quad \sqrt{(M_1^4 + M_e^4)(M_2^2 + M_e^2)^2 + 2M_1^2M_e^2(M_2^4 - 6M_2^2M_e^2 + M_e^4)}\Big] \\
M_{\ell\ell q}^{\min} &= 271.8\,\mathrm{GeV}
\end{aligned} \tag{2}$$

where

$$M_q = M_{\tilde{q}_L},\ M_2 = M_{\tilde{\chi}_2^0},\ M_e = M_{\tilde{\ell}_R},\ M_1 = M_{\tilde{\chi}_1^0}\,.$$

In order to extract $M_{\ell\ell q}^{\min}$, events were selected as before with the additional requirement $M_{\ell\ell} > M_{\ell\ell}^{\max}/\sqrt{2}$, corresponding to $z > 0$, and the larger of the two possible $\ell\ell q$ masses formed by combining the lepton pair with the two highest p_T jets was chosen. This distribution is shown in Figure 4. The lower edge is not very sharp, presumably because gluon radiation can carry off energy and so give masses below the nominal end point. Nevertheless, the lower edge is clearly visible and is not obscured by the kinematic cuts.

A fit to the shape including a Gaussian resolution where the width was allowed to float is unstable; as the fit range was changed the value of the width changed significantly and was sometimes unreasonably large. This effect seems to be due to the small tail below the edge. Therefore, the Gaussian width was constrained to be 10% of the edge value ($M_{\ell\ell q}^{\mathrm{low}}$). This width was used to smear the form

$$[A(M - M_{\ell\ell q}^{\mathrm{low}}) + B(M - M_{\ell\ell q}^{\mathrm{low}})^2]\theta(M - M_{\ell\ell q}^{\mathrm{low}})$$

which was then fitted to the distribution allowing A, B and $M_{\ell\ell q}^{\mathrm{low}}$ to float. The fit gives $M_{\ell\ell q}^{\mathrm{low}} = 283.7^{+4.4}_{-4.5}\,\mathrm{GeV}$. The χ^2 for the fit is rather poor (30 for 11 degrees of freedom), mainly because of the few bins around 200 GeV; a better fit can be obtained by restricting the range to $300 - 600\,\mathrm{GeV}$. Because of this, and because the edge is not very sharp, more study with different choices of the SUSY parameters is needed to understand the actual error on the fitted value that could be achieved. We shall assume conservatively in the discussion below (see Section 7) that an error of $\pm 2\%$ can be achieved.

There is also a minimum value of the hq invariant mass from the decay chain $\tilde{q}_L \to \tilde{\chi}_2^0 q \to \tilde{\chi}_1^0 hq$. If the jet is again treated as massless, this is given by

$$\begin{aligned}
(M_{hq}^{\min})^2 &= \tfrac{1}{2M_2^2}(M_q^2 - M_2^2)\times \\
&\Big[(M_2^2 + M_h^2 - M_1^2) - \sqrt{(M_2^2 - M_h^2 - M_1^2)^2 - 4M_1^2M_h^2}\Big] \\
M_{hq}^{\min} &= 346.5\,\mathrm{GeV}
\end{aligned} \tag{3}$$

It has been shown previously that the Higgs decay to $b\bar{b}$ [6, 2] can be extracted. The following cuts were applied

- $M_{\mathrm{eff}} > 400\,\mathrm{GeV}$;
- $\not{E}_T > \max(100\,\mathrm{GeV}, 0.2M_{\mathrm{eff}})$;
- at least four jets with $p_T > 50\,\mathrm{GeV}$ and one with $p_{T,1} > 100\,\mathrm{GeV}$;

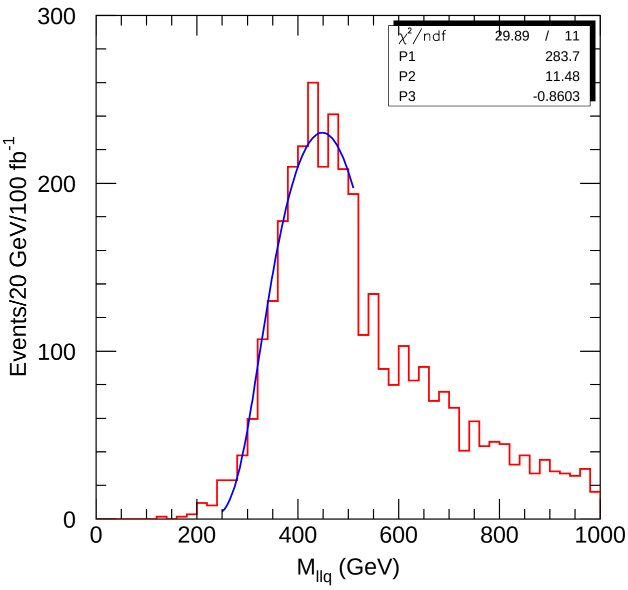

Figure 4: Distribution of the larger of the two $\ell\ell q$ masses after cuts described in the text, showing the lower edge.

- Transverse sphericity $S_T > 0.2$.

In addition, events were selected to have exactly two b jets with $p_{T,b} > 25\,\mathrm{GeV}$, $70 < M_{bb} < 110\,\mathrm{GeV}$, and the larger of the two masses formed by combining this pair with either of the two hardest jets was selected, since at least one of the two should be greater than the minimum mass. This distribution is shown in Figure 5. While there is a threshold in roughly the right place, it is not very distinct. This probably is due to a combination of resolution for this multijet system and of the substantial combinatorial background under the Higgs peak. A side-band subtraction and careful jet energy calibration might be able to clean up the distribution. We will assume below an error of $\pm 5\%$; this is substantially larger than the $\ell\ell q$ error and will only add a very weak additional constraint. It would be important to study this further in cases where the decay to sleptons is not available such as "Point 1" and "Point 2" of Refs. 2 and 3.

4 Model-independent masses

In this section we discuss how the measurements in the previous section and those discussed previously [2, 6] can be used to determine the masses of the SUSY particles without reference to the underlying SUGRA model. The identification of the decay chains is needed but these are based on much weaker assumptions. We have a number of measurements all related to the process $\tilde{q}_L \to \tilde{\chi}_2^0 \to \tilde{\ell}_R \to \tilde{\chi}_1^0$:

- $M_{\ell\ell}^{\max} = \left[\frac{(M_2^2 - M_{\tilde{\ell}_R}^2)(M_{\tilde{\ell}_R}^2 - M_1^2)}{M_{\tilde{\ell}_R}^2}\right]^{1/2} = 108.9 \pm 0.11\,\mathrm{GeV}$ (see Ref [2])

- $M_{\ell\ell q}^{\max} = \left[\frac{(M_{\tilde{q}_L}^2 - M_{\tilde{\chi}_2^0}^2)(M_{\tilde{\chi}_2^0}^2 - M_{\tilde{\chi}_1^0}^2)}{M_{\tilde{\chi}_2^0}^2}\right]^{1/2} = 552.4 \pm 5.5\,\mathrm{GeV}$

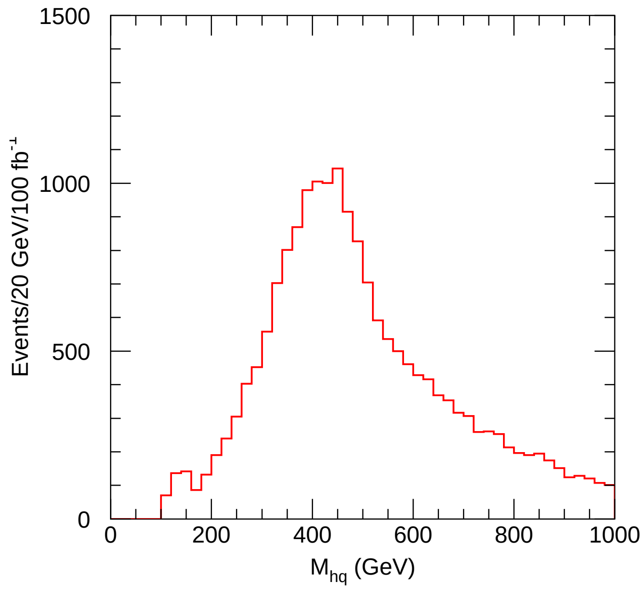

Figure 5: Larger of the two $b\bar{b}q$ jet masses, showing the hq mass threshold.

- $M_{\ell q}^{\max} = \left[\frac{(M_{\tilde{q}_L}^2 - M_{\tilde{\chi}_2^0}^2)(M_{\tilde{\chi}_2^0}^2 - M_{\tilde{\ell}_R}^2)}{M_{\tilde{\chi}_2^0}^2}\right]^{1/2} = 479.3 \pm 5.5\,\mathrm{GeV}$
- $M_{\ell\ell q}^{\min}$ (Equation 2) $= 271.8 \pm 5.4\,\mathrm{GeV}$

There are also two measurements related to $\tilde{\chi}_2^0 \to \tilde{\chi}_1^0 h$:

- The maximum hq mass (see Reference 2)

$$(M_{hq}^{\max})^2 = M_h^2 + \left(M_{\tilde{q}}^2 - M_{\tilde{\chi}_2^0}^2\right)\left[\frac{M_{\tilde{\chi}_2^0}^2 + M_h^2 - M_{\tilde{\chi}_1^0}^2 + \sqrt{(M_{\tilde{\chi}_2^0}^2 - M_h^2 - M_{\tilde{\chi}_1^0}^2)^2 - 4M_h^2 M_{\tilde{\chi}_1^0}^2}}{2M_{\tilde{\chi}_2^0}^2}\right].$$

  which has the value $M_{hq}^{\max} = 522.6 \pm 5.2\,\mathrm{GeV}$.

- The minimum hq mass $M_{hq}^{\min}$ (Equation 3) $= 346.5 \pm 17.3\,\mathrm{GeV}$

A large error is assigned to the hq lower edge because it is not sharp and there is a lot of background (see above).

If the lower edges discussed in the previous section are ignored, there are four measurements and four unknown masses masses $M_{\tilde{q}_L}$, $M_{\tilde{\chi}_2}$, $M_{\tilde{\ell}_R}$ and $M_{\tilde{\chi}_1^0}$. Nevertheless, for the errors assumed there is a one-parameter family of solutions labeled by $M_{\tilde{\chi}_1^0}$, with small uncertainties in the other masses for a fixed value of $M_{\tilde{\chi}_1^0}$. This remains true even if the errors are substantially reduced.

If the lower edges are included, then all four masses can be determined. The errors were estimated numerically as follows. The $\tilde{q}_L$, $\tilde{\chi}_2^0$, and $\tilde{\ell}_R$ masses were generated uniformly within $\pm 50\%$ of their nominal values, and the $\tilde{\chi}_1^0$ mass was calculated using the dilepton edge ($M_{\ell\ell}$), which has a much smaller error than the other measurements. The χ^2 for the remaining measurements was calculated, and the point was assigned a probability of $\exp(-\chi^2/2)$. The resulting distributions are shown in Figure 6. The resulting errors range from $\pm 12\%$ for the mass of $\tilde{\chi}_1^0$ to $\pm 3\%$ for the

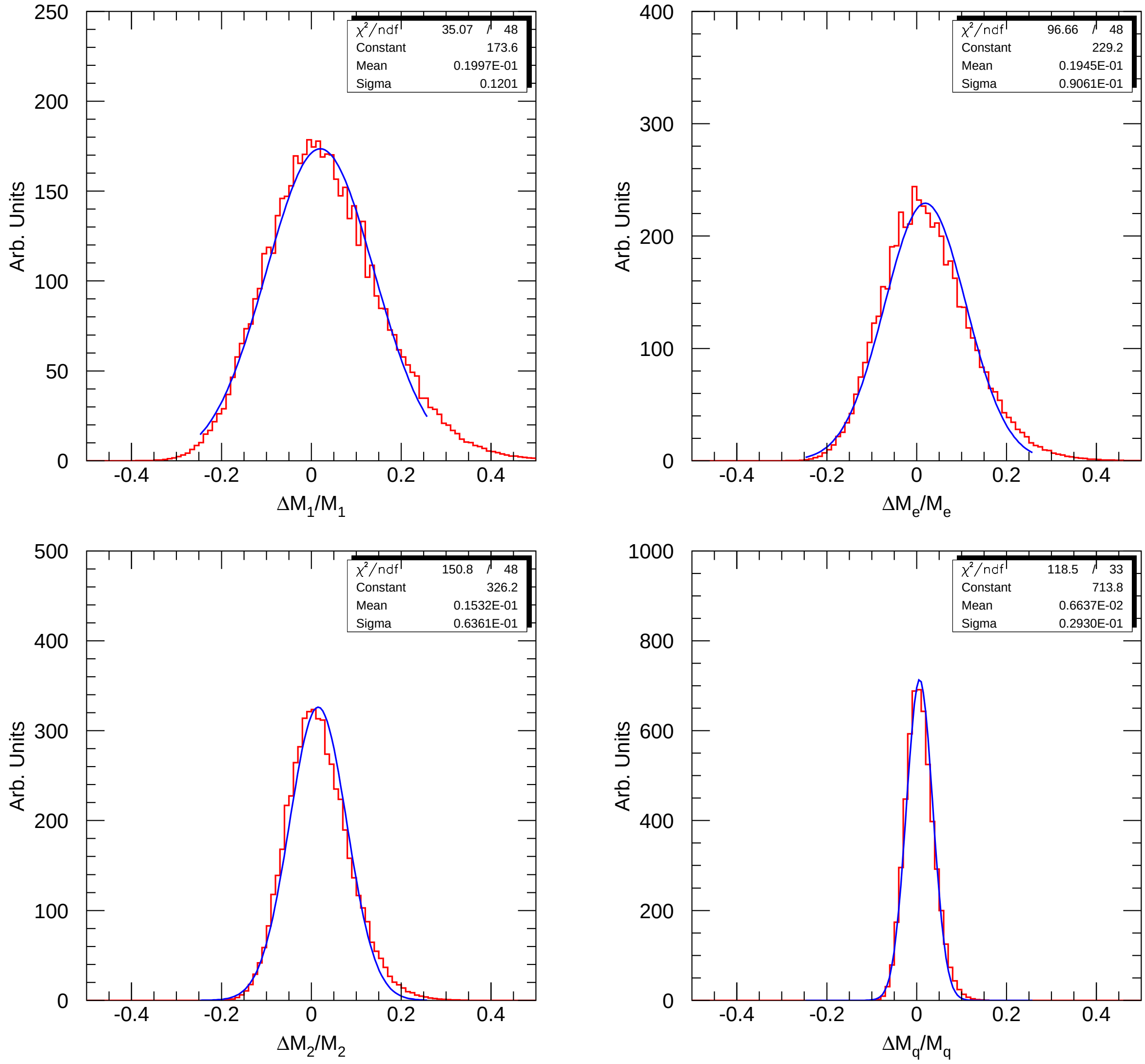

Figure 6: Distribution of the $\tilde\chi_1^0$, $\tilde\ell_R$, $\tilde\chi_2^0$, and $\tilde q_L$ masses satisfying all constraints discussed in the text. The fitted widths are about $\pm12\%$, $\pm9\%$, $\pm6\%$, and $\pm3\%$ respectively.

mass of $\tilde q_L$. If the error on $M_{\ell\ell q}^{\rm min}$ were reduced to $\pm1\%$, as might be possible with a more careful understanding of the systematics, the error on $M_{\tilde\chi_1^0}$ would be reduced to $\pm7.5\%$. The errors are highly correlated as can be seen from Figures 7–8 which show the scatter plots of $M_{\tilde\chi_2^0}$ *vs.* $M_{\tilde\chi_1^0}$ and $M_{\tilde\ell_R}$ vs. $M_{\tilde\chi_1^0}$. Of course, the errors on the masses are much poorer than those that arise from a fit within the SUGRA model (see Section 7 and Ref. [2]), but they do not involve any model assumptions.

5 Dilepton measurement errors

In order to provide significant constraints on model parameters and tests of the underlying model a number of measurements with *comparable* errors are needed. In general, measuring one combination of SUSY masses very precisely is not particularly useful if the other combinations involve jets and

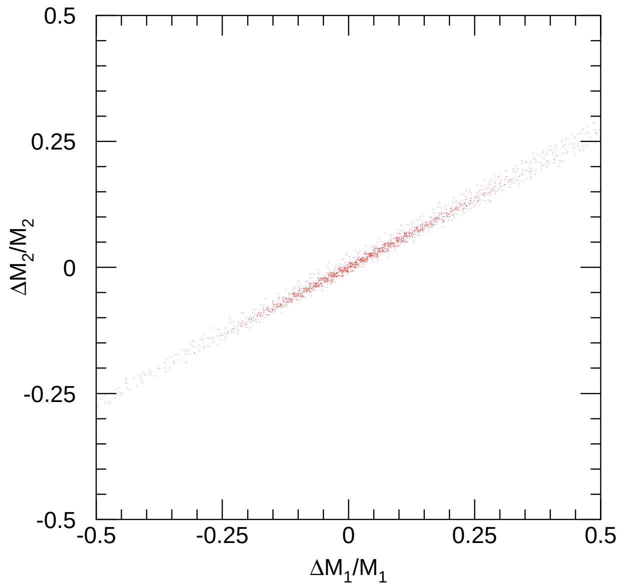

Figure 7: Scatter plot of $M_{\tilde{\chi}_2^0}$ vs. $M_{\tilde{\chi}_1^0}$ solutions satisfying all constraints discussed in the text.

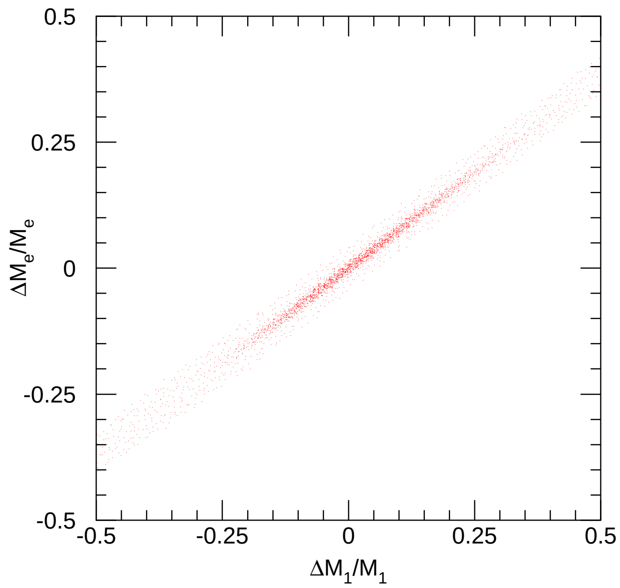

Figure 8: Scatter plot of $M_{\tilde{\ell}_R}$ vs. $M_{\tilde{\chi}_1^0}$ solutions satisfying all constraints discussed in the text.

so are only measured with an accuracy of several percent. An important exception is the decay $\tilde{\chi}_2^0 \to \tilde{\ell}_R^\pm \ell^\mp \to \tilde{\chi}_1^0 \ell^+ \ell^-$, which has an end point at

$$M_{\ell\ell}^{\max} = M_{\tilde{\chi}_2^0} \sqrt{1 - \frac{M_{\tilde{\ell}_R}^2}{M_{\tilde{\chi}_2^0}^2}} \sqrt{1 - \frac{M_{\tilde{\chi}_1^0}^2}{M_{\tilde{\ell}_R}^2}} \,. \tag{4}$$

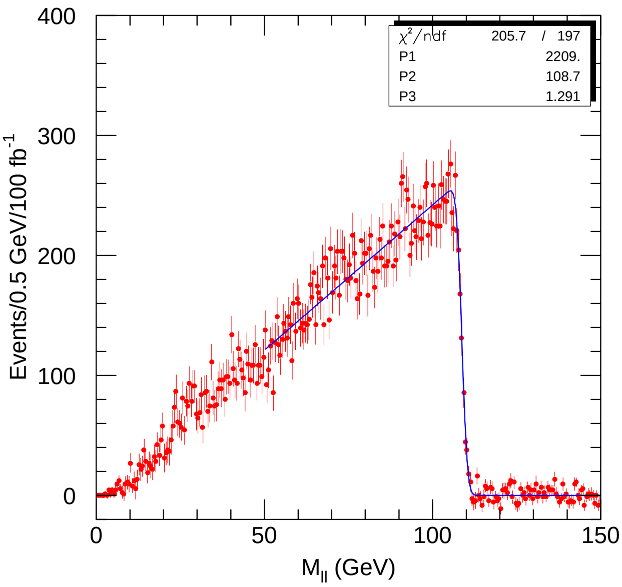

Figure 9: $\ell^+\ell^-$ mass distribution showing the χ^2 MINUIT fit using PAW.

A difference in the end points for e^+e^- and $\mu^+\mu^-$ would directly indicate a difference in the $\tilde{e}_R$ and $\tilde{\mu}_R$ masses, which obviously an important issue for testing models that purport to understand flavor physics. This decay is generally allowed in SUGRA models which give cosmologically interesting cold dark matter [13], such as the one discussed here. It is also common in GMSB models since the $\tilde{\ell}_R$ has only $U(1)$ couplings and tends to be light. The derivative of the end-point with respect to $M_{\tilde{\ell}_R}$ vanishes at the geometric mean of the $\tilde{\chi}_1^0$ and $\tilde{\chi}_2^0$ masses but in general is of order one; for the masses in the case studied here,

$$\frac{dM_{\ell\ell}^{\max}}{dM_{\tilde{\ell}_R}} = 0.478\,.$$

The same sample of 10^6 SUSY events was used to estimate how well such an edge might be measured with full LHC luminosity. In the absence of cuts, the mass distribution should be given by the same formula as discussed in Section 2, namely

$$(M_{\ell\ell}^{\max})^2 \frac{1+z}{2} dz$$

with z uniformly distributed. This form was smeared with a Gaussian using numerical integration as in Section 2. Figures 9 and 10 show the resulting fits using MINUIT with either the χ^2 or the maximum likelihood method; the parameters are the overall normalization, the end point, and the Gaussian width. The fitted end points with errors from MINOS [11] are $108.71^{+0.087}_{-0.088}$ GeV and $108.60^{+0.065}_{-0.060}$ GeV respectively. The fits are consistent with each other, but neither quite agrees within errors with the expected end point at 108.92 GeV. The statistical errors are slightly better than the systematic errors expected from the lepton energy scale [12] and are comparable to the errors on the W mass expected to be achieved ultimately at the Tevatron [14] and LEP [15].

The maximum $|\eta_\ell|$ for the either of the two leptons is plotted in Figure 11 and peaks around $\eta_{\max} = 1$. Thus both the barrel and the endcap regions of the detector are important. If precise electron and muon measurements were available only in the barrel, about half the events would be lost.

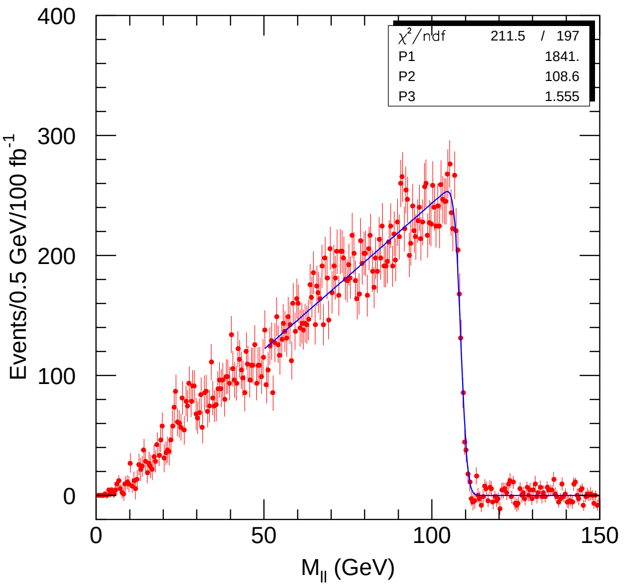

Figure 10: $\ell^+\ell^-$ mass distribution showing the maximum likelihood MINUIT fit using PAW.

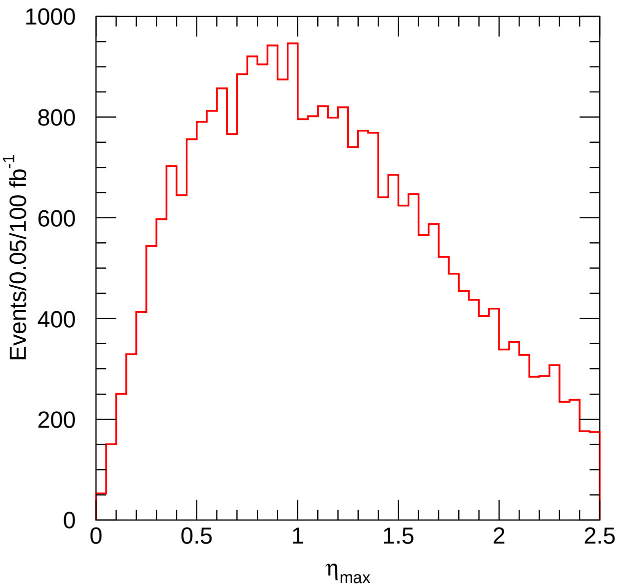

Figure 11: Maximum $|\eta_\ell|$ for dilepton events.

Clearly a lot more work is needed to understand how to calibrate the detector and to extract information at this level of accuracy. In particular, the discrepancy between the fitted and calculated end points even in this highly idealized simulation needs to be understood, presumably by studying many different samples of SUSY events. It seems clear, however, that statistical errors below about 0.1% may be achievable, especially if the masses were a bit lower so that the $\tilde{\chi}_2^0 \to \tilde{\chi}_1^0 h$ decay were absent.

6 Non-minimal SUGRA models

The case studied so far assumes that the scalar masses are all equal at the GUT scale, an assumption that is rather restrictive and may not be valid. By studying variations in this assumption, we can try to estimate howl the various LHC signals are modified and how well this assumption could be tested. We shall show that qualitatively new signals emerge in our preliminary study of non-universal SUGRA (NUSUGRA) models which is carried out using two kinds of NUSUGRA models closely related to the SUGRA case discussed above.

6.1 Variations of masses with $SU(5)$ representations

We vary the scalar masses at the unification scale by assuming that squarks and sleptons which are in the **10** of SU(5) have a common scalar mass m_{10} while those that are in the **5** of SU(5) have a mass m_5. Here, m_{10} is kept at its nominal value of 100 GeV while m_5 is shifted. Two points have been studied in detail, namely $m_5 = 75\,\mathrm{GeV}$ and $m_5 = 125\,\mathrm{GeV}$. The masses of the superpartners at these points are given in Table 1. Squark masses are almost insensitive to these changes in m_5; the shifts are much smaller than the errors that were obtained in Section 4 because $m_{1/2}$ plays a dominant role in these masses via the strong coupling of squarks. The significant changes take place in the slepton spectrum, in particular in the masses of $\tilde{\ell}_L$. Samples of 200000 events were simulated for each of the new cases; 10^6 Standard Model background events were also used to ensure that the cuts are effective in disposing of it.

6.1.1 The $m_5 < 100\,\mathrm{GeV}$ case

In the benchmark case, $m_5 = m_{10} = 100\,\mathrm{GeV}$, the decay sequence $\tilde{\chi}_2^0 \to \tilde{\ell}_R^\pm \ell^\mp \to \tilde{\chi}_1^0 \ell^+ \ell^-$ is allowed, giving a very clear signature: the lepton pair invariant mass distribution presents a sharp edge near the kinematic limit, Equation 4. For modified points with $m_5 < 85\,\mathrm{GeV}$, the left handed slepton becomes lighter than $\tilde{\chi}_2^0$ thus the decay sequence $\tilde{\chi}_2^0 \to \tilde{\ell}_L^\pm \ell^\mp \to \tilde{\chi}_1^0 \ell^+ \ell^-$ is also allowed, giving rise to a second edge at

$$M_{\ell\ell}^{\prime\max} = M_{\tilde{\chi}_2^0} \sqrt{1 - \frac{M_{\tilde{\ell}_L}^2}{M_{\tilde{\chi}_2^0}^2}} \sqrt{1 - \frac{M_{\tilde{\chi}_1^0}^2}{M_{\tilde{\ell}_L}^2}} \approx 34.9\,\mathrm{GeV} \ \text{ for } \ m_5 = 75\,\mathrm{GeV}\,.$$

The position of the edge is sensitive to $M_{\tilde{\ell}_L}$ and thus to m_5. As there is less available phase space in this decay than in the decay to ℓ_R, these leptons are softer and it is necessary to lower the cuts as much as possible to ensure good acceptance. ATLAS expects to be able to detect muons down to $p_T = 5\,\mathrm{GeV}$, so the following selection cuts are applied:

- $M_{\mathrm{eff}} > 800\,\mathrm{GeV}$;
- $\not{E}_T > 0.2 M_{\mathrm{eff}}$;
- at least one $R = 0.4$ jet with $p_T > 100\,\mathrm{GeV}$;
- $\ell^+\ell^-$ pair with $|\eta_\ell| < 2.5$, $p_{T,e} > 10\,\mathrm{GeV}$, and $p_{T,\mu} > 5\,\mathrm{GeV}$;
- ℓ isolation cut: $E_T < 10\,\mathrm{GeV}$ in $R = 0.2$ around the leptons;
- Transverse sphericity $S_T > 0.2$.

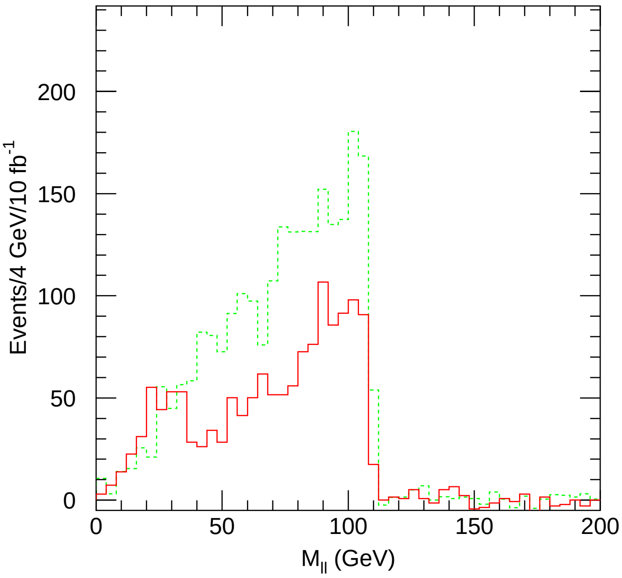

Figure 12: $M_{\ell\ell}$ distribution after the cuts at the $m_5 = m_{10} = 100\,\mathrm{GeV}$ point (dashed line) and modified point with $m_5 = 75\,\mathrm{GeV}$ (solid line).

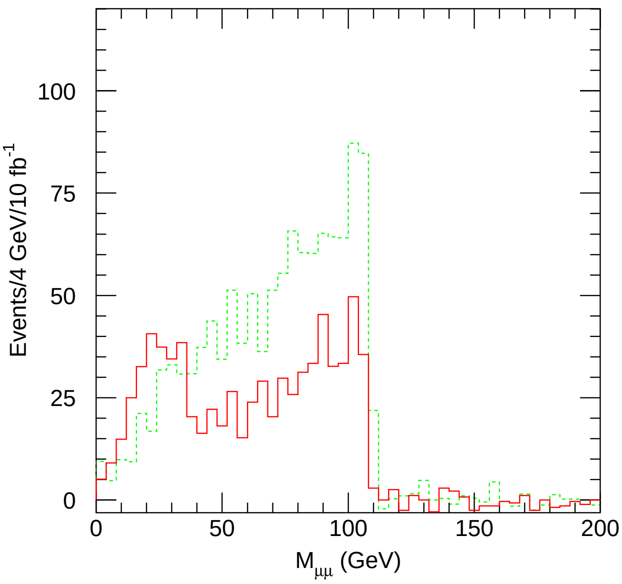

Figure 13: $M_{\mu\mu}$ distribution after the cuts at the $m_5 = m_{10} = 100\,\mathrm{GeV}$ point (dashed line) and modified point with $m_5 = 75\,\mathrm{GeV}$ (solid line).

Figures 12 and 14 show the lepton pair invariant mass for the benchmark case and the modified cases with $m_5 = 75\,\mathrm{GeV}$ and $m_5 = 50\,\mathrm{GeV}$. Figures 13 and 15 show the muon pair invariant mass for the same cases. The edge at low $M_{\ell\ell}$ for $m_5 = 75\,\mathrm{GeV}$ is clearer in the muon case due to the increased acceptance at low p_T. The presence of two structures with comparable rates enables one to deduce the presence of two decay chains and to measure the two end points. Notice that as m_5

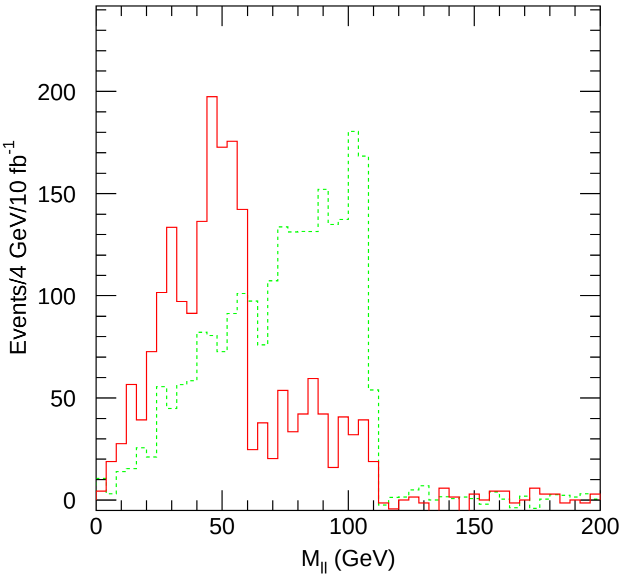

Figure 14: $M_{\ell\ell}$ distribution after the cuts at the $m_5 = m_{10} = 100\,\text{GeV}$ point (dashed line) and modified point with $m_5 = 50\,\text{GeV}$ (solid line).

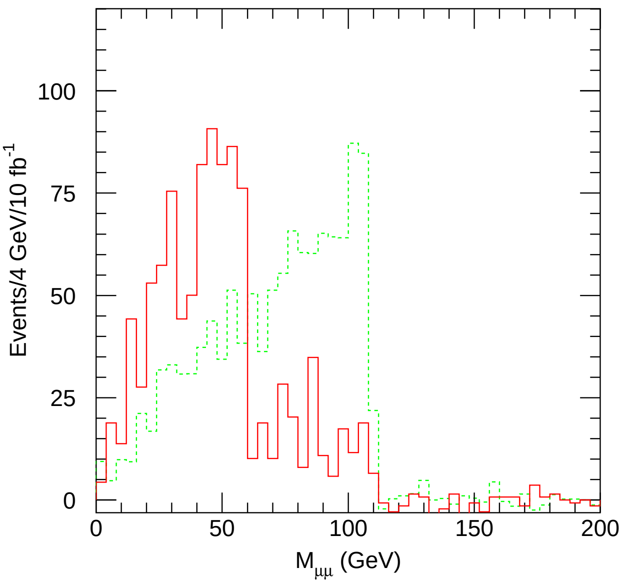

Figure 15: $M_{\mu\mu}$ distribution after the cuts at the $m_5 = m_{10} = 100\,\text{GeV}$ point (dashed line) and modified point with $m_5 = 50\,\text{GeV}$ (solid line).

is reduced to 50 GeV, the higher mass structure is becoming weaker because the $\tilde{\chi}_2^0 \ell \tilde{\ell}_L$ coupling is larger than the $\tilde{\chi}_2^0 \ell \tilde{\ell}_R$ one. As m_5 increases, $M_{\tilde{\ell}_L}$ increases, and the branching ratio for $\tilde{\chi}_2^0 \to \ell \tilde{\ell}_L$ vanishes quickly around $m_5 = 80$ GeV. Hence, $m_5 = 75\,\text{GeV}$ is about the upper limit where one can distinguish from the benchmark case using this channel.

6.1.2 The $m_5 > 100\,\text{GeV}$ case

In this case there is no visible effect on the $\ell^+\ell^-$ distribution or any of the other distributions studied in the previous sections. Production of $\tilde{\ell}_L$ via the decay of strongly interacting sparticles is small, so one must rely on direct production via the Drell-Yan process. It is possible [6] to extract a signal for Drell-Yan production with $\tilde{\ell}_L \to \tilde{\chi}_1^0 \ell$ by requiring two isolated leptons, missing energy, and no jets, but the slepton mass can only be inferred from the rate and kinematic distributions. The jet veto is essential to elliminate events with leptons arising from the decays of squarks and gluinos.

If m_5 is somewhat larger than 100 GeV, the ℓ_L becomes heavy enough that the decay $\tilde{\ell}_L \to \tilde{\chi}_2^0 \ell$ is allowed. Then the decay chain

$$\begin{array}{lll} \tilde{\ell}_L & + & \tilde{\ell}_L \\ \downarrow & & \downarrow \\ \tilde{\chi}_1^0 + \ \ell^\pm & & \tilde{\chi}_2^0 + \ell^\mp \\ & & \downarrow \\ & & \tilde{\ell}_R + \ell'^\pm \\ & & \downarrow \\ & & \tilde{\chi}_1^0 + \ell'^\mp \end{array}$$

results in a final state with four isolated leptons. The signature is two same flavor opposite charge (SFOC) lepton pairs and no jet activity. In order to select these events, the following cuts were applied:

- no jet with $p_T > 40\,\text{GeV}$ and $|\eta| < 5$;
- at least 4 leptons with $p_T > 10\,\text{GeV}$ and $|\eta| < 2.5$ forming 2 SFOC pairs;
- the invariant mass of at least one of the pairs is less than 109 GeV (so that it is a candidate to arise from the decay of $\tilde{\chi}_2^0$);
- ℓ isolation cut: $E_T < 10\,\text{GeV}$ in $R = 0.2$ around the lepton.

The invariant mass of the three leptons coming from the same left-handed slepton provides information about its mass. The three leptons were selected as follows:

- a pair with invariant mass smaller than 109 GeV is assumed to come from the $\tilde{\chi}_2^0$ decay;
- the remaining lepton with lowest p_T is assumed to come from the same left handed slepton as the pair.

The invariant mass of the trilepton system is then computed. As the production rate is small, high luminosity is needed and an integrated luminosity of $300\,\text{fb}^{-1}$, representing the ultimate that can be achieved at LHC, was assumed. The $M_{\ell\ell\ell}$ invariant mass should have an upper limit given by:

$$M_{\ell\ell\ell}^{\max} = \sqrt{\left(1 - \frac{M_{\tilde{\ell}_R}^2}{M_{\tilde{\chi}_2^0}^2}\right)\left(M_{\tilde{\ell}_L}^2\left(1 - \frac{M_{\tilde{\chi}_2^0}^2}{M_{\tilde{\ell}_L}^2}\right) + M_{\tilde{\chi}_2^0}^2\left(1 - \frac{M_{\tilde{\chi}_1^0}^2}{M_{\tilde{\ell}_R}^2}\right)\right)}$$

which is approximately 128.0 GeV for $m_5 = 125\,\text{GeV}$.

Figures 16, 17 and 18 show the tri-lepton invariant mass respectively at point 5, and the cases with $m_5 = 115\,\text{GeV}$, and $m_5 = 125$ GeV. As $M_{\tilde{\ell}_L}$ increases, the $\tilde{\ell}_L \to \tilde{\chi}_2^0 \ell$ branching ratio increases (2% for point 5, 10% for $m_5 = 125\,\text{GeV}$). A clear signal appears for $m_5 = 115\,\text{GeV}$. We estimate

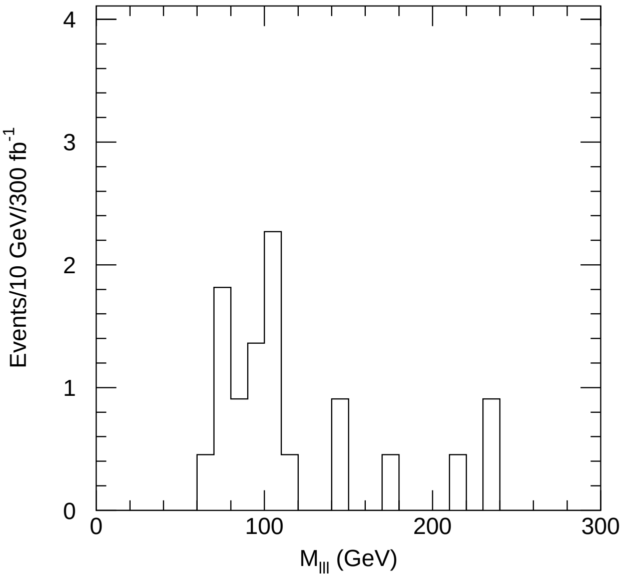

Figure 16: $M_{\ell\ell\ell}$ distribution after the cuts for the $m_5 = m_{10} = 100\,\mathrm{GeV}$ point. Note that the number of events is very small.

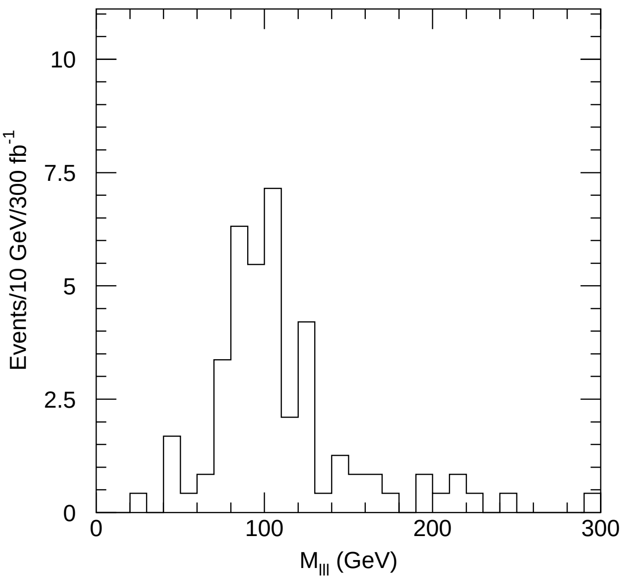

Figure 17: $M_{\ell\ell\ell}$ distribution after the cuts for the modified point with $m_5 = 115$ GeV.

that for masses larger than this, the position of the edge can be measured with a precision of 3 GeV and is very sensitive to m_5. As m_5 increases further, the production rate falls off and the signal disappears for m_5 above 250 GeV.

6.2 Variations of masses for the third generation

Here we investigate the possibility that m_0 for the third generation squarks and sleptons is different from that for the first two generations. As in the m_5 cases, the greatest sensitivity to this change is in the slepton sector, so we are forced to consider the detection of final states containing taus.

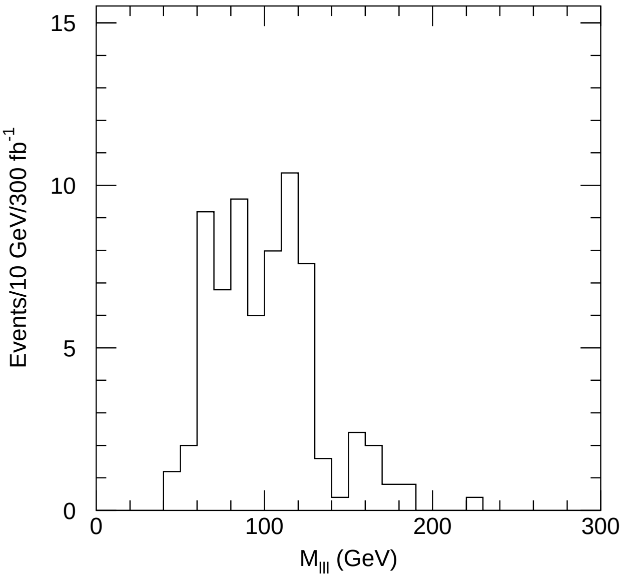

Figure 18: $M_{\ell\ell\ell}$ distribution after the cuts for the modified point with $m_5 = 125$ GeV.

In another study [16], the use of hadronic tau decays was illustrated. It was shown how the $\tau\tau$ invariant mass distribution could be inferred from the observed decay products and the kinematic end point extracted. This method enables $m_{\tilde{\tau}_R}$ to be constrained. If this method could be exploited in the case of interest here, slepton universality could be tested with great accuracy. The method fails for several reasons all of which are related to the observable event rate and background.

- The signal is less clear because the channels $\tilde{\chi}_2^0 \to h^0\tilde{\chi}_1^0$ and $\tilde{\chi}_2^0 \to \tilde{\ell}_R\ell$, ℓ being e or μ, are open here, whereas the $\tilde{\chi}_2^0$ decays only to staus for the case studied in Ref. 16. The decay to h also generates $\tau\tau$ final states at a comparable rate and distorts the shape of the distribution.
- Because the gluinos and squarks are heavier, the total SUSY cross section for the cases discussed here is smaller than in the case studied in Ref [16], resulting in smaller event samples for the same integrated luminosity.

Figure 19 shows the $\tau\tau$ invariant mass reconstructed from the visible decay products for our benchmark case after the following selection cuts are applied:

- $\not{E}_T > 0.2M_{\rm eff}$ or $> 100\,{\rm GeV}$;
- at least one $R = 0.4$ jet with $p_T > 100\,{\rm GeV}$;
- at least three additional $R = 0.4$ jets with $p_T > 50\,{\rm GeV}$;
- two jets identified as hadronic tau decays according to the methods described in Ref. 16.

The distribution is shown for the subtracted combination $\tau^+\tau^- - \tau^\pm\tau^\pm$ as this is reduces the background from jets that are misidentified as taus.

A sample of 100000 events have been generated; the plot is normalized to $10\,{\rm fb}^{-1}$, which would correspond to corresponding to ~ 230000 events so the statistical fluctuations are somewhat bigger than they would be in the actual experiment. The signal, of about 40 events in the bin at 50 GeV, is completely buried by the statistical fluctuations. Even several years of data taking at low

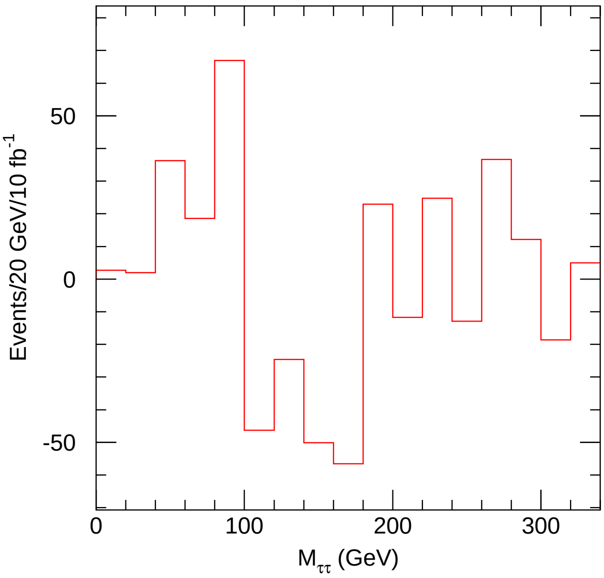

Figure 19: $M_{\tau^+\tau^-}$ distribution at point 5 after the cuts and after subtraction of same sign pairs.

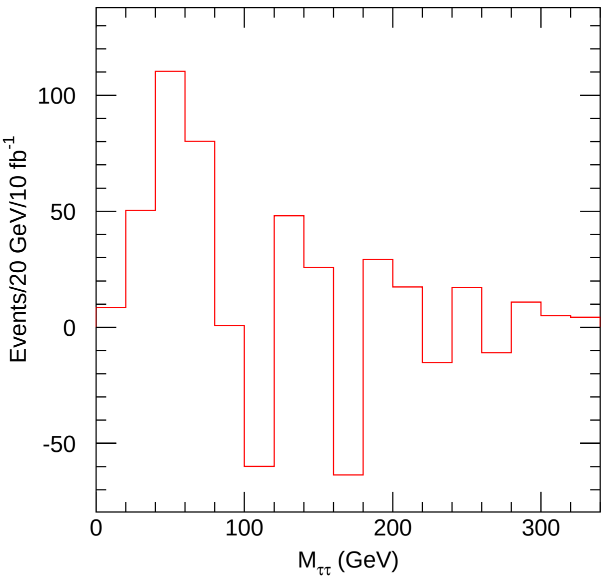

Figure 20: $M_{\tau^+\tau^-}$ distribution at modified point with $tan\beta = 5$ (other parameters at their nominal point 5 value) after the cuts and after subtraction of same sign pairs.

luminosity would not be enough to reduce them to a satisfying level. LHC high luminosity would give enough statistics, but the $M_{\tau\tau}$ reconstruction method used here is based on full simulation [17] and has not been proven to be viable at high luminosity; additional pile-up events could compromise it.

To emphasize the deterioration of the signal due to the $\tilde{\chi}_2^0 \to h^0\tilde{\chi}_1^0$ channel, a model with $\tan\beta$ shifted from 2.1 to 5 (the other SUGRA parameters remaining at their nominal values) has been

Table 2: Masses of the relevant superpartners, in GeV, in the default case and at modified points with $m_{3rd} = 30$, 70, 150 and 200 GeV. The first and second generation of squarks and sleptons are degenerate and so are not listed separately.

Sparticle	default	$m_{3rd} = 30$ GeV	$m_{3rd} = 70$ GeV	$m_{3rd} = 150$ GeV	$m_{3rd} = 200$ GeV
$\widetilde{g}$	769	769	769	769	769
$\widetilde{u}_l$	687	687	687	687	687
$\widetilde{u}_r$	664	664	664	664	664
$\widetilde{t}_1$	496	491	493	501	510
$\widetilde{t}_2$	706	701	704	712	721
$\widetilde{\chi}_1^{\pm}$	231	232	232	233	234
$\widetilde{\chi}_2^{\pm}$	514	514	515	533	549
$\widetilde{\chi}_1^0$	122	122	122	122	122
$\widetilde{\chi}_2^0$	232	233	233	234	235
$\widetilde{e}_L$	239	239	239	239	239
$\widetilde{e}_R$	157	157	157	157	157
$\widetilde{\nu}_e$	230	230	230	230	230
$\widetilde{\tau}_1$	124	157	140	193	234
$\widetilde{\tau}_2$	219	239	228	264	295
$\widetilde{\nu}_\tau$	209	230	219	256	288

studied. Since h^0 is now heavier, this decay channel is closed and the rate of tau pair production is 3 times greater. Figure 20 shows that the excess of $\tau^+\tau^-$ pairs now becomes visible; there are approximately 120 signal events in the plot concentrated in the bin at 50 GeV.

An alternative method of extracting evidence for excess τ-pair production based on leptonic final states is now illustrated. The method is similar to that of Ref [18]. In order to illustrate its sensitivity, we have studied models in which the SUGRA parameters remain at their nominal values except that the third generation squark and slepton masses (namely t_l, b_r, t_r, L_l, L_r) are set equal to m_{3rd} at GUT scale. The masses of the relevant superpartners for several values of m_{3rd} are given in Table 2, from which it can be seen that the largest effect is in the stau masses: as m_{3rd} increases the taus masses rise and the branching ratio for $\tilde{\chi}_2^0 \to \tau\tilde{\tau}_1$ is reduced. The channel closes for $m_{3rd} > 200\,\mathrm{GeV}$.

Samples of 200000 SUSY events were generated in each case shown in the table, (except for $m_{3rd} = 30\,\mathrm{GeV}$ and $200\,\mathrm{GeV}$ where 100000 events were generated). The Standard Model background has been added using a 1 million event sample. The only significant background after applying our selections is from $t\bar{t}$ events. In order to select SUSY events with slepton pair, and reject Standard Model background, the following cuts have been applied:

- $M_{\rm eff} > 500\,\mathrm{GeV}$;
- $\not{E}_T > \max(0.2M_{\rm eff}, 250\,\mathrm{GeV})$;
- at least one $R = 0.4$ jet with $p_T > 100\,\mathrm{GeV}$;
- at least four $R = 0.4$ jets with $p_T > 50\,\mathrm{GeV}$;
- $\ell\ell$ pair with $p_{T,\ell} > 10\,\mathrm{GeV}$, $|\eta_\ell| < 2.5$, ℓ being electron or muon;

Table 3: Ratios of production rates for lepton pairs for the five models studied (see text)

m_{3rd}	30 GeV	70 GeV	100 GeV (point 5)	150 GeV	200 GeV
$r_{OC} = \frac{e^+e^- + \mu^+\mu^-}{e^\pm\mu^\mp}$	2.61	3.86	3.99	4.62	4.38
$r_{SC} = \frac{e^\pm e^\pm + \mu^\pm\mu^\pm}{e^\pm\mu^\pm}$	0.88	0.79	1.25	1.05	1.01

- ℓ isolation cut: $E_T < 10\,\mathrm{GeV}$ in $R = 0.2$;

After these cuts the signal exceeds the Standard Model background by more than a factor of ten; the background is mainly due to top quark pair production. Lepton pairs in the signal events arise mainly from two processes.

- The decay of χ_2^0, via $\tilde{\chi}_2^0 \to \tilde{\ell}^\pm \ell^\mp \to \tilde{\chi}_1^0 \ell^+ \ell^-$ where $\tilde{\ell}$ is $\tilde{e}_R$, $\tilde{\mu}_R$, $\tilde{\tau}_1$, or $\tilde{\tau}_2$; ℓ is the corresponding lepton. This channel produces exclusively oppositely (OC) pairs, of the same flavor (SFOC) in case of selectrons or smuons, and both same (SFOC) and opposite flavor (OFOC) pairs in case of leptons from resulting from leptonic tau decays.

- The decay of a $\tilde{\chi}_1^\pm$ pair, produced in the decays of gluinos: even if the $\tilde{g} \to \tilde{\chi}_1^\pm qq$ branching ratio is small, this channel is important since it can produce same charge (SC) pairs, as gluinos are Majorana fermions. The flavors of the leptons are uncorrelated. The main $\tilde{\chi}_1^\pm$ decay modes are: $\tilde{\chi}_1^\pm \to \tilde{\chi}_1^0 W^\pm \to \tilde{\chi}_1^0 \ell^\pm \nu_\ell(\bar{\nu}_\ell)$ $\tilde{\chi}_1^\pm \to \tilde{\chi}_1^0 \ell^\pm \nu_\ell$ $\tilde{\chi}_1^\pm \to \tilde{\nu}_\ell \ell^\pm$, ℓ being e, μ or τ.

A violation of e, μ, τ universality will be revealed by comparing the number of events containing same flavor lepton pair (SF), with the number of events containing opposite flavor lepton pair (OF). Define

$$r_{OC} = \frac{e^+e^- + \mu^+\mu^-}{e^\pm\mu^\mp}$$

This ratio decreases as the branching ratio for $\tilde{\chi}_2^0 \to \tilde{\tau}\tau$ increases. The second class of processes listed above is sensitive to violations of $e\mu$ universality only and consequently r_{SC} defined for same charge lepton pairs is independent of violations of e, τ universality.

Table 3 and Figure 21 show r_{OC} and r_{SC} for different values of m_{3rd} The error bars shown on Figure 21 correspond to 10 fb^{-1} of integrated luminosity. r_{SC} is insensitive to violations of e/μ universality and should be the same for all the cases considered. The errors indicated on Figure 21 show that the apparent differences are statistical fluctuations.

In the region between the benchmark case and $m_{3rd} = 70\,\mathrm{GeV}$, the contribution to r_{OC} from the second class of processes decreases dramatically since, at $m_{3rd} = 70\,\mathrm{GeV}$, $\tilde{\nu}_\tau$ becomes significantly lighter than $\tilde{\chi}_1^\pm$, and the decay mode $\tilde{\chi}_1^\pm \to \tilde{\nu}_\tau \tau$ becomes important, with a branching ratio of 30% instead of 0.4%, to the detriment of decays to electrons and muons. For $m_{3rd} \sim 75\,\mathrm{GeV}$, $\tilde{\tau}_2$ becomes lighter than $\tilde{\chi}_2^0$ (see table 2), and the decay channel $\tilde{\chi}_2^0 \to \tilde{\tau}_2 \tau$, opens resulting in a large violation of e/τ universality and increasing the number of OFOC pairs. For $75\,\mathrm{GeV} < m_{3rd} < 100\,\mathrm{GeV}$, very slight change in the ratios is to be expected, since these channels are not open, and the branching ratios of the usual channel $\tilde{\chi}_2^0 \to \tilde{\ell}\ell$ changes only slowly. For $m_{3rd} > 100$ GeV the only interesting decay mode is $\tilde{\chi}_2^0 \to \tilde{\ell}\ell$: as $m_{\tilde{\tau}_1}$ increases and tends to $m_{\tilde{\chi}_2^0}$, the decay branching ratio $\tilde{\chi}_2^0 \to \tilde{\tau}\tau$ closes, and r_{OC} increases. The channel closes at $m_{3rd} = 200\,\mathrm{GeV}$.

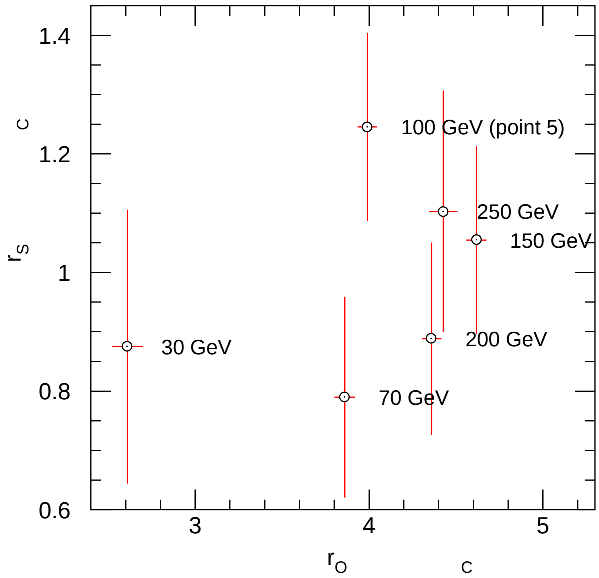

Figure 21: r_{OC} and r_{SC} for various m_{3rd} values (see text). The error bars correspond to an integrated luminosity of 10 fb^{-1}.

To summarize: for $m_{3rd} < 100\,\mathrm{GeV}$, r_{OC} is very sensitive to m_{3rd}. If $10\,\mathrm{GeV} < m_{3rd} < 75\,\mathrm{GeV}$, one should be able to constrain it with an accuracy of a few GeV. For $m_{3rd} > 100\,\mathrm{GeV}$, things are not so easy: for ($m_{3rd} < 200\,\mathrm{GeV}$), r_{OC} increases slightly, giving some sensitivity to its value. As a result, models with m_{3rd} above 200 GeV can hardly be distinguished from each other.

7 Determination of parameters

In previous studies [2, 6] we needed to rely on a global fit to a specific model, e.g., minimal SUGRA, to determine individual masses from the combinations of masses measured by various end points. The analysis in Section 4 allows us to extract masses in a rather general way, but the global fit is still useful. Since the measurements in Sections 2 and 3 provide new information, we reevaluate here the precision with which the model parameters can be determined. The strategy is the same as before: the parameter space of the SUGRA model is searched using random sampling in order to determine the $\pm 34\%$ confidence limits resulting from the assumed "experimental" quantities and their estimated errors.

The following quantities and estimated errors are used in the fit:

$$
\begin{aligned}
(M_{hq}^{\max})^2 &= M_h^2 + \left(M_{\tilde{q}}^2 - M_{\tilde{\chi}_2^0}^2\right)\left[\frac{M_{\tilde{\chi}_2^0}^2 + M_h^2 - M_{\tilde{\chi}_1^0}^2 + \sqrt{(M_{\tilde{\chi}_2^0}^2 - M_h^2 - M_{\tilde{\chi}_1^0}^2)^2 - 4M_h^2 M_{\tilde{\chi}_1^0}^2}}{2M_{\tilde{\chi}_2^0}^2}\right], \\
&= (552.6 \pm 40\,\mathrm{GeV})^2\,; \\
M_{\ell\ell}^{\max} &= M_{\tilde{\chi}_2^0}\sqrt{1 - \frac{M_{\tilde{\ell}}^2}{M_{\tilde{\chi}_2^0}^2}}\sqrt{1 - \frac{M_{\tilde{\chi}_1^0}^2}{M_{\tilde{\ell}}^2}} = 108.9 \pm 0.1\,\mathrm{GeV}\,; \\
R = \frac{M_{\ell q}^{\max}}{M_{\ell\ell q}^{\max}} &= \sqrt{\frac{M_{\tilde{\chi}_2^0}^2 - M_{\ell_R}^2}{M_{\tilde{\chi}_2^0}^2 - M_{\tilde{\chi}_1^0}^2}} = 0.865 \pm 0.02\,;
\end{aligned}
$$

$$
\begin{aligned}
M_{\ell q}^{\max} &= \sqrt{\frac{(M_{q_l}^2 - M_{\tilde\chi_2^0}^2)(M_{\tilde\chi_2^0}^2 - M_{\ell_R}^2)}{M_{\tilde\chi_2^0}^2}} = 478.1 \pm 40\,\mathrm{GeV}\,; \\
(M_{\ell\ell q}^{\min})^2 &= \frac{1}{4M_2^2 M_e^2}\Big[-M_1^2 M_2^4 + 3M_1^2 M_2^2 M_e^2 - M_2^4 M_e^2 - M_2^2 M_e^4 - M_1^2 M_2^2 M_q^2 - \\
&\quad M_1^2 M_e^2 M_q^2 + 3M_2^2 M_e^2 M_q^2 - M_e^4 M_q^2 + (M_2^2 - M_q^2) \times \\
&\quad \sqrt{(M_1^4 + M_e^4)(M_2^2 + M_e^2)^2 + 2M_1^2 M_e^2 (M_2^4 - 6M_2^2 M_e^2 + M_e^4)}\Big]\,, \\
&= (271.8 \pm 5.4\,\mathrm{GeV})^2\,; \\
(M_{hq}^{\min})^2 &= \frac{1}{2M_2^2}(M_q^2 - M_2^2) \times \\
&\quad \Big[(M_2^2 + M_h^2 - M_1^2) - \sqrt{(M_2^2 - M_h^2 - M_1^2)^2 - 4M_1^2 M_h^2}\Big]\,, \\
&= (346.5 \pm 17\,\mathrm{GeV})^2\,.
\end{aligned}
$$

In addition we include M_h in the fit with an error of $\pm 3\,\mathrm{GeV}$. The experimental error on the mass from $h \to \gamma\gamma$ will be considerably less than this. The error reflects our estimate of the theoretical uncertainty in relating the Higgs mass to the parameters of the SUGRA model.

A fit of the minimal SUGRA model to these inputs results in the following values of the parameters:

- $m_0 = 100.0 \pm 3.63$ GeV,
- $m_{1/2} = 300.0 \pm 4.99$ GeV,
- $\tan\beta = 2.11 \pm 0.18$,
- $\mu = +1$;

The errors are symmetric, unlike the earlier fits. Recall that we previously [2] quoted:-

- $m_0 = 100^{+12}_{-8}$ GeV,
- $m_{1/2} = 300^{+6}_{-4}$ GeV,
- $\tan\beta = 1.8^{+0.3}_{-0.5}$,
- $\mu = +1$;

Thus the new measurements improve the fit to the minimal SUGRA model as well as allowing masses to be extracted without assuming the model.

A completely general model at the GUT scale would have as many parameters as the MSSM. To keep the problem tractable, we consider three variants of the SUGRA model, each with only one additional parameter. We use the same fitting procedure to estimate how well these additional parameters could be constrained if the actual data corresponded to the benchmark case, *i.e.* we estimate how well we can actually constrain to SUGRA model.

We first allow the values of m_0 at GUT scale to be different for the two Higgs representations. Restricting $m_{H_d}^2 = m_{H_d}^2 = m_{h-GUT} > 0$, leads to a 5-parameter fit and the following result (m_0 is now the common mass for all the other scalars)

- $m_0 = 100 \pm 3.68$ GeV,
- $m_{1/2} = 301 \pm 5.94$ GeV,
- $\tan\beta = 2.11 \pm .18$,
- $\mu = +1$;
- $m_{h-GUT} < 430$ GeV, 95% confidence

The insensitivity to m_{h-GUT} arises because the derived value of μ is large (~ 500 GeV) and the value of m_{H_U} (the Higgs doublet that couples to charge 2/3 quarks) at the weak scale is determined mainly by the top quark Yukawa coupling and stop mass and not by the value of m_{H_U} at the GUT scale (m_{h-GUT}). Therefore the masses of $\tilde{\chi}_1^0$, $\tilde{\chi}_2^0$ and h are insensitive to m_{h-GUT} unless it is very large. If the H and A Higgs bosons (and the heaviest gauginos) could be observed and their masses measured m_{H_U} could be constrained. The masses of these particles vary by ~ 40 GeV for parameters in the allowed range. The production rates for these particles at LHC are extremely small and their discovery is probably not possible there. This insensitivity to m_{h-GUT} is quite general [19].

We next split the squark and slepton masses at the unification scale: the particles that are in the **10** of SU(5) are assumed to have common scalar mass m_{10} and those that lie in **5** of SU(5) are assumed to have common scalar mass m_5. Fitting for these, we get

- $m_{10} = 100 \pm 3.8$ GeV,
- $m_{1/2} = 300^{+10}_{-7}$ GeV,
- $\tan\beta = 2.11 \pm .23$,
- $\mu = +1$;
- $m_5 < 420$ GeV, 95% confidence

The lack of precise constraints on these new parameters can be understood. Since $m_{1/2}$ is significantly larger than m_0, the values of the squark masses at low energy are controlled by $m_{1/2}$. The excellent constraint on m_{10} arises because it controls m_{ℓ_R} which is very precisely determined by the $\ell^+\ell^-$ end point. $\tilde{\ell_L}$ would be observable if the decay $\tilde{\chi}_2^0 \to \tilde{\ell_L}\ell \to \ell^+\ell^-\tilde{\chi}_1^0$ were open as discussed in Section 6.1.1. The failure to observe this decay then constrains m_{ℓ_L} and consequently m_5. Adding this constraint excludes the region $m_5 < 75 GeV$. Direct production of right handed sleptons excludes the region $m_5 > 115$ GeV although this difficult search requires high luminosity as explained in Section 6.1.2. Using these constraints we infer:

- $m_5 = 100^{+6}_{-10}$ GeV.

Finally, we consider the case where the third generation squark and slepton masses at the GUT scale are allowed to vary. As can be seen from Table 2, the sensitivity is confined to the stau masses so that a fit without the information from Section 6.2 results in almost no constraint on m_{3rd}. The errors on the other parameters are as above. Adding the constraints from this section implies that

- $m_{3rd} = 100^{-8}_{+4}$ GeV.

8 Conclusions

In this paper we have demonstrated a number of new techniques that could be used to determine masses and decay properties of supersymmetric particles at the LHC. We have shown that cascade decays with several steps can be used to reconstruct the masses of supersymmetric partilces without any knowledge of the underlying model. We have illustrated new signals that appear when the SUGRA model is extended to have more parameters and have shown in particular how e/τ universality could be tested. We have further demonstrated the very high precision with which many of these parameters can be constrained.

Acknowledgements

This work was supported in part by the Director, Office of Science, Office of Basic Energy Research, Division of High Energy Physics of the U.S. Department of Energy under Contracts DE-AC03-76SF00098 and DE-AC02-98CH10886. Accordingly, the U.S. Government retains a nonexclusive, royalty-free license to publish or reproduce the published form of this contribution, or allow others to do so, for U.S. Government purposes.

Appendix: Attempt at complete reconstruction of SUSY events

The three-step decay chain $\tilde{q}_L \to \tilde{\chi}_2^0 \to \tilde{\ell}_R \to \tilde{\chi}_1^0$ provides three mass constraints using the values determined in Section 4 and so a $0C$ fit for the $\tilde{\chi}_1^0$ momentum is possible. If the same decay is selected on both sides of the event, then, in principle, one could completely reconstruct the event using $\not{E}_T$ to select the best solution. This method was successful for GMSB models [8] with decays involving leptons and photons, but it fails in this case due to the experimental resolution, as we will now show.

Events were selected to be consistent with two $\tilde{\chi}_2^0 \to \tilde{\ell}^\pm \ell^\mp \to \tilde{\chi}_1^0 \ell^+ \ell^-$ decays and so to have four leptons, at least two jets, and missing energy:

- $M_{\text{eff}} > 400\,\text{GeV}$.
- $\not{E}_T > \max(0.2 M_{\text{eff}}, 100\,\text{GeV})$.
- At least two jets with $p_{T,1} > 100\,\text{GeV}$, $p_{T,2} > 75\,\text{GeV}$ and at least two charged tracks in $R = 0.4$.
- Four isolated leptons with $p_T > 10\,\text{GeV}$, $\eta < 2.5$. Isolation being defined so that there is less than 10 GeV of additional transverse energy in a cone $R = 0.2$ around the lepton direction.

The cut on the charged multiplicity of the jets was made to eliminate electrons and hadronic tau decays from the jet sample. It was further required that there be one and only one way to form two opposite-sign, same-flavor pairs of the four leptons with $20\,\text{GeV} < M_{\ell\ell} < 115\,\text{GeV}$. This ensures an unambiguous paring of the leptons consistent with two $\tilde{\chi}_2^0$ decays.

The events were then fit to the hypothesis that the four leptons and the two highest p_T jets came from the $\tilde{q}_L \to \tilde{\chi}_2^0 \to \tilde{\ell} \to \tilde{\chi}_1^0$ decay chain. For each such decay chain there are three mass constraints, namely

$$(p_{\tilde{\chi}_1^0} + p_{\ell,1})^2 = M_{\tilde{\ell}}^2$$

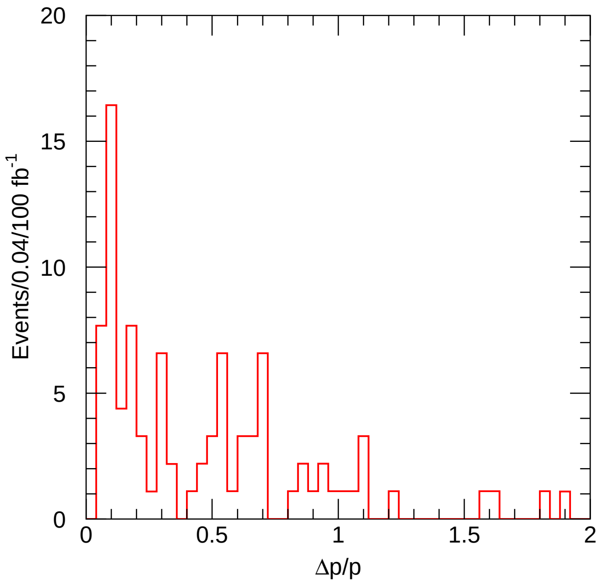

Figure 22: difference $\Delta p/p$ between the generated and the best reconstructed $|\vec{p}|$.

$$\begin{aligned}(p_{\tilde{\chi}_1^0} + p_{\ell,1} + p_{\ell,2})^2 &= M^2_{\tilde{\chi}_2^0} \\ (p_{\tilde{\chi}_1^0} + p_{\ell,1} + p_{\ell,2} + p_q)^2 &= M^2_{\tilde{q}}\end{aligned}$$

There are also two constraints from $\not{E}_T$. Since the measurement errors on the jets are comparable to those on $\not{E}_T$, the jet energies were smeared by factors λ_i distributed in Gaussian manner, and the best solution was taken to be the one which minimizes

$$\chi^2 = \frac{(\not{E}_x - p_{1x} - p_{2x})^2}{\sigma^2(\not{E}_x)} + \frac{(\not{E}_y - p_{1y} - p_{2y})^2}{\sigma^2(\not{E}_y)} + \frac{\lambda_1^2}{\sigma^2(\lambda_1)} + \frac{\lambda_2^2}{\sigma^2(\lambda_2)},$$

where both the missing energy resolutions $\sigma(\not{E}_{x,y})$ and the jet energy scale resolutions $\sigma(\lambda_{1.2})$ are determined using the Gaussian calorimeter resolution. The resulting difference $\Delta p/p$ between the generated and the best reconstructed $|\vec{p}|$ for the $\tilde{\chi}_1^0$ is shown in Figure 22. A similar reconstruction was successful in the case of the GMSB study [8] where the decay chain

$$\tilde{\chi}_2^0 \to \tilde{\ell}^\pm \ell^\mp \to \tilde{\chi}_1^0 \ell^\pm \ell^\mp \to \tilde{G}\gamma\ell^\pm\ell^\mp$$

was used. The reconstruction works much more poorly than in the GMSB case; while a few events are correctly reconstructed, most are not. This is not very surprising; the GMSB case relied on leptons and photons which have much better energy resolution than the jets used here. In addition, in this case, the $\tilde{\chi}_1^0$ momenta are significantly smaller than the jet momenta and so the errors on the jet energy measurements are very important.

References

[1] L. Alvarez-Gaume, J. Polchinski and M.B. Wise, Nucl. Phys. **B221**, 495 (1983);
L. Ibañez, Phys. Lett. **118B**, 73 (1982);
J.Ellis, D.V. Nanopolous and K. Tamvakis, Phys. Lett. **121B**, 123 (1983);

K. Inoue *et al.* Prog. Theor. Phys. **68**, 927 (1982);
A.H. Chamseddine, R. Arnowitt, and P. Nath, Phys. Rev. Lett., **49**, 970 (1982).

[2] I. Hinchliffe, F.E. Paige, M.D. Shapiro, J. Söderqvist, and W. Yao, Phys. Rev. **D55**, 5520-5540 (1997).

[3] E. Richter-Was, D. Froidevaux, and J. Söderqvist, ATLAS Internal Note PHYS-No-108 (1997).

[4] I. Hinchliffe, F.E. Paige, E. Nagy, M.D. Shapiro, J. Söderqvist, and W. Yao, ATLAS Internal Note PHYS-No-109 (1997).

[5] F. Gianotti, ATLAS Internal Note PHYS-No-110 (1997).

[6] G. Polesello, L. Poggioli, E. Richter-Was, and J. Söderqvist, ATLAS Internal Note PHYS-No-111 (1997).

[7] M. Dine, W. Fischler and M. Srednicki, Nucl. Phys. **B189**, 575 (1981);
S. Dimopoulos and S. Raby, Nucl. Phys. **B192,** 353 (1981);
C. Nappi and B. Ovrut, Phys. Lett.**113B,** 175 (1982);
L. Alvarez-Gaumé, M. Claudson and M. Wise, Nucl. Phys. **B207,** 96 (1982);
M. Dine and A. Nelson, Phys. Rev. **D48**, 1227 (1993);
M. Dine, A. Nelson and Y. Shirman, Phys. Rev. **D51,** 1362 (1995);
M. Dine, *et al.*, Phys. Rev. **D53,** 2658 (1996).

[8] I. Hinchliffe and F.E. Paige, hep-ph/9812233 (December, 1998).

[9] S. Kuhlman, et al., *Physics and Technology of the Next Linear Collider: A Report Submitted to Snowmass '96*, BNL-52502 (1996).

[10] H. Baer, F.E. Paige, S.D. Protopopescu, and X. Tata, hep-ph/9804321 (1998).

[11] F. James, CERN Program Library Long Writeup D506 (1998).

[12] ATLAS DETECTOR AND PHYSICS PERFORMANCE TECHNICAL DESIGN REPORT, Chapter 12, CERN/LHCC 99-15.

[13] J. Ellis, *et al.*, Nucl. Phys. **B238**, 453 (1984);
A. Gabutti *et. al.,* hep-ph/9602432;
H. Baer and M. Brhlik, Phys. Rev. **D53**, 597 (1996).

[14] B.Abbott *et.al.*, Phys. Rev. Lett. **80**, 3000 (1998), Phys. Rev. **D 58**, 092003 (1998); F. Abe *et al.*, Phys. Rev. **D52**, 4784,1995, Y.-K. Kim, talk at La Thuile 5 March 1999.

[15] DELPI collaboration Eur. Phys. J. **C2**, 581 (1998); ALEPH Collaboration, Phys. Lett. **B453**, 121 (1999); L3 Collaboration, L3 preprint-171, Phys. Lett. (to appear); OPAL Collaboration, CERN-EP/98-197, Phys. Lett. (to appear).

[16] I. Hinchliffe and F. Paige ATLAS Internal Note ATL-COM-PHYS-99-018.

[17] Y. Coadou *et al.*, ATLAS Internal Note ATL-PHYS-98-126.

[18] S. Abdullin and D. Denegri, hep-ph/9905510.

[19] N. Kersting, private communication.